

# Vanadium(IV) complexes with picolinic acids in NaY zeolite cages

## Synthesis, characterization and catalytic behaviour

Alexander Kozlov,<sup>a</sup> Kiyotaka Asakura,<sup>b</sup> and Yasuhiro Iwasawa<sup>a\*†</sup>

<sup>a</sup> Department of Chemistry, Graduate School of Science, The University of Tokyo, Hongo, Bunkyo-ku, Tokyo 113, Japan

<sup>b</sup> Research Center for Spectrochemistry, Faculty of Science, The University of Tokyo, Hongo, Bunkyo-ku, Tokyo 113, Japan

Encapsulated vanadium picolinic complexes have been synthesized by treatment of a dehydrated form of VO<sup>2+</sup>-NaY zeolite with molten picolinic acids and characterized by X-ray photoelectron spectroscopy (XPS), extended X-ray absorption fine structure (EXAFS), X-ray absorption near-edge structure (XANES), EPR, FTIR and UV–VIS spectroscopies, and XRD. It was suggested by XRD and XPS that the complexes were located in the zeolite cavities. Differences in the spectroscopic properties of encapsulated and impregnated samples were explained in terms of coordination of vanadium complexes with zeolite –OH groups. The stability of VO(pic)<sub>2</sub> and its adduct with pyridine depended strongly on the complex location. The encapsulated vanadium picolinate complex retained solution-like activity in the liquid-phase oxidation of hydrocarbons and alcohols with hydrogen peroxide.

The great expansion in the study of acidic and bifunctional catalysis over zeolites<sup>1</sup> has led to a variety of technological applications for petrochemical reactions. However, there is much less information available for catalytic systems where zeolite-based materials act as redox catalysts. In the last decade there has been significant interest in the design of redox molecular sieves and considerable progress has been made in their use in liquid-phase oxidations.<sup>1–3</sup> Two routes, involving isomorphous substitution of transition metal ions in the lattice of zeolites or encapsulation of transition metal complexes in zeolite voids can be applied to prepare redox zeolite catalysts.<sup>4–7</sup> The first method dictates occupation of the regular tetrahedral framework sites by metal cations. The requirements imposed by coordination chemistry, as well as those derived from zeolite synthesis procedure, often make it difficult to modify the metal specification in these materials, resulting in a slight change in catalytic behaviour. However, the second method provides the opportunity of physical entrapment of metal complexes in an ordered matrix and allows one to avoid both covalent and ionic attachment to the solid support. Generally, so called ‘ship-in-a-bottle’ catalysts can have the combined property of solution-like activity and shape selectivity.<sup>8,9</sup>

Since Romanovsky *et al.* reported the synthesis and catalysis of encapsulated metal phthalocyanate complexes in NaY zeolite in 1977,<sup>10</sup> a variety of encapsulated complexes have been synthesized and characterized. However, studies have concentrated on epoxidation catalysis and only a few publications have been concerned with alkane and benzene hydroxylation reactions.

The ability of vanadium complexes to activate reduced forms of oxygen is well known and numerous applications to a variety of hydrocarbon oxidations have been reported in homogeneous systems.<sup>11–13</sup> The balance between heterolytic and homolytic oxygen transfer is strongly influenced by the type of ligands coordinated to vanadium. Recently, encapsulated VO(salen)-NaY and VO(bipy)<sub>2</sub>-NaY catalysts have been reported, which showed activity for cyclohexene and cyclo-

hexane oxidations.<sup>14,15</sup> Immobilization of metal complexes with enhanced homolytic reactivity, such as vanadium complexes with pyridine- and pyrazine-carboxylic acids,<sup>16</sup> was not successful until our recent study<sup>17</sup> which reported the synthesis of vanadium complexes with picolinic acid encapsulated in Y-zeolite supercages.

In the present paper we extend our previous study to vanadium complexes with substituted picolinic acids in NaY zeolite. We also report detailed characterization of the structure of the vanadium species by XPS, EXAFS, XANES, EPR, FTIR and UV–VIS spectroscopies. Location of the complexes is also discussed based on XPS and XRD data.

## Experimental

### Materials

The starting vanadium compound VOSO<sub>4</sub> · nH<sub>2</sub>O (*n* = 3–4) (purity 99.9%) and special grade solvents were purchased from Wako Pure Chemical Industries. Picolinic acid (picH) (99%), quinaldic acid (QpicH) (99%), 5-*n*-butyl-2-picolinic acid (BupicH) (95%) were received from Soekawa Chemicals. Urea hydrogen peroxide addition compound (98%, Aldrich) was used as an oxidant. The authentic samples for gas chromatographic analysis (all EP grade) were received from Soekawa Chemicals. NaY zeolite with an Si/Al ratio of 5.6 was supplied by Tosoh Company (HSZ-320NAA, Lot. 3001) and pretreated before use by a literature method.<sup>18</sup>

### Sample preparation

**VO(pic)<sub>2</sub> · H<sub>2</sub>O.** Vanadium(IV) complexes with picolinic acids were synthesized in a similar manner to that reported in ref. 19. 100 ml of 0.4 mol l<sup>-1</sup> aqueous solution of VOSO<sub>4</sub> (8.68 g) was added to 250 ml of 0.16 mol l<sup>-1</sup> hot (333 K) aqueous solution of picH (9.84 g) within 1–2 min. 5% NH<sub>4</sub>OH was used to control the pH of the mixture at *ca.* 7. The mixture was stirred at 333 K for 1 h. A blue precipitate of the VO(pic)<sub>2</sub> · H<sub>2</sub>O formed and was filtered, washed with hot water, and dried in vacuum. C<sub>12</sub>H<sub>10</sub>N<sub>2</sub>O<sub>6</sub>V; Calc.: C 43.76%, H 3.04%, N 8.51%; found: C 42.88%, H 3.17%, N 8.35%.

† E-mail: iwasawa@utsc.s.u-tokyo.ac.jp

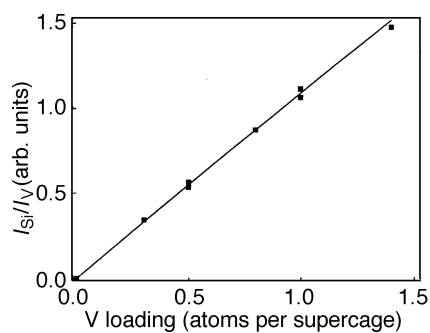


**Fig. 1** Calibration plot for quantification of vanadium in zeolites constructed with VO(acac)<sub>2</sub>-NaY impregnated samples

**VO<sup>2+</sup>-NaY.** 5 g of a hydrated form of NaY zeolite was ion exchanged with 100 ml of 0.05 mol l<sup>-1</sup> aqueous solution of VOSO<sub>4</sub> for 10 h.<sup>20</sup> The resultant mixture was filtered and washed twice with 50 ml of water. All the procedures were performed under argon (99.9999% purity) atmosphere. The VO<sup>2+</sup>-NaY was dried in vacuum at 298 K for 4 h, followed by evacuation at 503 K for 2 h. The resultant VO<sup>2+</sup>-NaY zeolite was used as a precursor for a 'ship-in-a-bottle' type synthesis without storage.

**Encapsulated VO(pic)<sub>2</sub>-NaY (SB).** 4 g of the VO<sup>2+</sup>-NaY zeolite precursor was treated with 10 g of molten picH at 433 K for 6 h under an argon atmosphere. The sample was then Soxhlet extracted with pyridine for 60 h and dried in vacuum for 4 h at 298 K. The sample was further heated at 413 K for 10 h in a He flow to remove adsorbed pyridine before use as a catalyst. The sample thus obtained is denoted as SB.

**Encapsulated VO(Bupic)<sub>2</sub>-NaY (SB) and VO(Qpic)<sub>2</sub>-NaY (SB).** These samples were prepared by a similar procedure to that described above for encapsulated VO(pic)<sub>2</sub>-NaY (SB) sample, except for prolonged time of complexation (10 h at 433 K).

**Impregnated VO(pic)<sub>2</sub>-NaY (IM).** A pyridine solution of VO(pic)<sub>2</sub>·H<sub>2</sub>O (0.36 g) was added to a suspension of 4 g VO<sup>2+</sup>-NaY zeolite in pyridine and the mixture was stirred at 353 K for 1 h. The pyridine was then allowed to evaporate under a fan at room temperature, followed by drying in vacuum for 4 h at 298 K and heating at 413 K for 10 h in a He flow.

**Impregnated VO(Bupic)<sub>2</sub>-NaY (IM) and VO(Qpic)<sub>2</sub>-NaY (IM).** These samples were prepared by a similar procedure to that described above for impregnated VO(pic)<sub>2</sub>-NaY (IM).

### Spectroscopic characterization

EPR spectra for powdered samples were obtained at room temperature on a JES-RE2X spectrometer. The microwave power was 1.00 mW with a resonance frequency of 9.1 GHz (X-band). The *g* values were determined relative to DPPH (*g* = 2.0036). Positions of *m*<sub>1</sub> = ±7/2 transitions and *m*<sub>1</sub> = ±5/2 transitions were used to estimate the *g* and *A* values. As a general rule the quadrupole term was ignored in interpretation of the EPR spectra.<sup>21</sup>

UV-VIS diffuse reflectance spectra in the region 250–900 nm were recorded on a Hitachi U-3500 spectrometer using a quartz cell for powdered samples at room temperature in air. A disk of NaY zeolite was used as a reference. FTIR spectra (resolution 2 cm<sup>-1</sup>) were recorded with a JASCO FT/IR-300E spectrometer using a self-supporting disk.

V K-edge XAFS spectra for the vanadium samples and a mixture of a reference compound and boron nitride, as self-

supporting disks, were measured at the BL-7C station of the Photon Factory in the National Laboratory for High Energy Physics (KEK-PF) with a positron energy of 2.5 GeV and a storage ring current 250–350 mA (Proposal No. 95G199). Synchrotron radiation was monochromatized by a Si(111) sagittal focusing double crystal. Higher harmonics were removed by using a total-reflection double mirror and detuning the parallelism for the intensity to 60% of the maximum. V K-edge spectra were recorded in a transmission mode using ionization chambers filled with flowing N<sub>2</sub> for *I*<sub>0</sub> and *I* as X-ray detectors. The EXAFS data were analysed by the EXAFS analysis program Rigaku EXAFS (REX).

Quantification of vanadium in samples was performed using energy dispersive X-ray fluorescence (XRF) on a Seiko SII SEA2010, equipped with a rhodium source for X-rays, a series of secondary targets and Si (Li) drift detector. Typical counting time was 100 s with dead time of 60–70% under excitation conditions of 50 kV and 12 mA. The ratio of the intensities of the vanadium peak to the silicon peak was plotted against the vanadium loading in Fig. 1 which was used to determine the vanadium content of the samples. The calibration curve was obtained by using NaY zeolites impregnated with given amounts of VO(acac)<sub>2</sub>.

XRD patterns were obtained using Ni filtered Cu-Kα radiation and the Rigaku computer-controlled instrument in 2θ–θ mode.

XPS were registered with a Rigaku XPS 7000 spectrometer using a monochromatic aluminum Kα<sub>1,2</sub> X-ray excitation source (1486.6 eV) and an X-ray power of 200 W (accelerating voltage 20 keV, current 10 mA) in an analysis chamber with a base pressure less than 5 × 10<sup>-7</sup> Pa. Samples were pressed into thin disks and placed in a pre-chamber, outgassed to less than 1 × 10<sup>-6</sup> Pa at room temperature, and then transferred to the analysis chamber. The binding energies were referred to 154.0 eV for the Si 2s level. The relative concentration (*n*<sub>1</sub>/*n*<sub>2</sub>) of two elements (1 and 2) was estimated by the following equation using Scofield's photoelectron cross-sections ( $\sigma_i$ ):<sup>22</sup>

$$n_1/n_2 = (I_1/I_2)(\sigma_2 \lambda_2 S_2/\sigma_1 \lambda_1 S_1)$$

where  $\sigma_1$ ,  $\sigma_2$  are the photoionization cross-sections;  $\lambda_1$ ,  $\lambda_2$  are the electron mean free paths and *S*<sub>1</sub>, *S*<sub>2</sub> are the analyser transmissions.

### Catalytic oxidation

Liquid-phase oxidation reactions were performed in thermostatted cylindrical vessels in air under vigorous stirring at 313 K. Addition of the catalyst was considered to be the starting point of the reaction. Reaction solutions were analysed by temperature-programmed GC chromatography using a 6 m column of 15% Unisole 30T on Uniport HP.

### Results and Discussion

Preparation of encapsulated vanadium complexes with picolinic acids consisted of three steps: (1) preparation of vanadium-modified zeolite as a precursor, (2) synthesis of encapsulated vanadium complexes by a flexible ligand method and (3) post-synthesis treatments. In the first step, NaY zeolite was ion exchanged with an aqueous solution of vanadyl sulfate followed by dehydration in vacuum at 368 or 503 K, resulting in VO<sup>2+</sup>-NaY zeolite precursor. The VO<sup>2+</sup>-NaY samples were partially dehydrated at 368 K and fully dehydrated at 503 K and exhibited EPR parameters *g*<sub>||</sub> = 1.937, *g*<sub>⊥</sub> = 1.998, *A*<sub>||</sub> = 192.9 G and *A*<sub>⊥</sub> = 79.0 G, and *g*<sub>||</sub> = 1.911, *g*<sub>⊥</sub> = 1.996, *A*<sub>||</sub> = 205.8 G and *A*<sub>⊥</sub> = 85.4 G, respectively (Table 1). In the present study the fully dehydrated VO<sup>2+</sup>-NaY zeolite was used. The choice of vanadium-modified zeolite is quite important for the synthesis. Obviously, complexation must occur from the outer parts of the zeolite

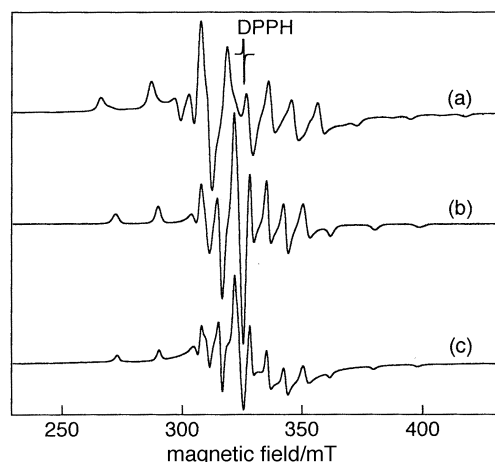
**Table 1** EPR parameters for selected NaY zeolite supported vanadium complexes

sample <sup>a</sup>	$g_{\perp}$	$g_{\parallel}$	$A_{\perp}/G$	$A_{\parallel}/G$
VO <sup>2+</sup> -NaY [368 K	1.998	1.937	79.0	192.9
dehydrated]503 K	1.996	1.911	85.4	205.8
VO(pic) <sub>2</sub> -NaY (SB)	1.996	1.945	67.1	175.3
VO(pic) <sub>2</sub> -NaY (IM)	1.994	1.947	66.1	174.1
VO(Bupic) <sub>2</sub> -NaY (SB)	1.995	1.942	69.3	180.1
VO(Qpic) <sub>2</sub> -NaY (SB)	1.996	1.942	71.5	182.3

<sup>a</sup> Except for VO<sup>2+</sup>-NaY and VO(pic)<sub>2</sub>-NaY (IM) the EPR parameters were taken for samples after Soxhlet extraction.

crystal toward the inner parts, where vanadium ions/species in zeolite would be required to have low mobility. In practice, V<sup>5+</sup>-NaY zeolite synthesized by a solid-state reaction and a hydrated form of ion exchanged VO<sup>2+</sup>-NaY zeolite did not produce encapsulated complexes. In other words, complexes were formed on the external surfaces of the zeolite and were removed by Soxhlet extraction similar to the impregnated materials. Redistribution of vanadium species is probably due to their high mobility from the inner to the external surface of the zeolite crystal. In consequence, use of zeolites modified with the less mobile V<sup>4+</sup>=O species was necessary. Dehydration of the ion-exchanged VO<sup>2+</sup>-NaY zeolite in vacuum at 503 K produced homogeneously distributed V<sup>4+</sup> species with low mobility, which were located on type III sites inside the zeolite supercage.<sup>20</sup> The dehydrated VO<sup>2+</sup>-NaY zeolite was found to be the best precursor for the synthesis of various encapsulated vanadium picolinate complexes by a flexible ligand method. All synthesis procedures, *i.e.* preparation of the VO<sup>2+</sup>-NaY zeolite precursor and the treatment with picolinic acids described below were performed under an argon atmosphere (99.9999% purity) to prevent V<sup>4+</sup>-species being oxidized and to minimize non-uniform vanadium redistribution by moisture. Moreover, formation of vanadium(v) species is undesirable because of the ability of vanadium(v) to catalyse hydrolysis of the NaY framework under the synthesis condition.<sup>23</sup>

In the second step (flexible ligand synthetic procedure), the VO<sup>2+</sup>-NaY was treated with molten picolinic or substituted picolinic acids. Complexation with picolinic acids was accompanied by a colour change from grey to greenish-brown. EPR spectra showed the gradual disappearance of the VO<sup>2+</sup>-NaY signal and the appearance of a new signal with parameters similar to those for an impregnated VO(pic)<sub>2</sub>-NaY sample ( $g_{\parallel} = 1.947$ ,  $g_{\perp} = 1.994$ ,  $A_{\parallel} = 174.1$  G, and  $A_{\perp} = 66.1$  G) (Fig. 2). Note that the high melting points of the picolinic acids (*e.g.* pyridine-2-carboxylic acid (picH) mp = 412–415 K) demand

**Fig. 2** EPR spectra of (a) VO<sup>2+</sup>-NaY zeolite, (b) VO(pic)<sub>2</sub>-NaY (SB), and (c) VO(pic)<sub>2</sub>-NaY (IM)

relatively severe synthesis conditions. During the high-temperature treatment formation of a small amount of CO<sub>2</sub>, due to ligand decarboxylation, was observed.

In the third step, the encapsulated vanadium samples were Soxhlet extracted with pyridine for 60 h. This was sufficient to remove most of the non-complexed ligand as well as vanadium picolinate located on the external surfaces of the zeolite (Table 2). The other solvents such as acetonitrile showed low efficiency for washing out surface-bound complexes. The Soxhlet-extracted samples contained much adsorbed pyridine that could significantly affect the spectroscopic and catalytic properties of the prepared materials. The samples were, therefore, further treated at 413 K for 12 h in a flow of He to remove the adsorbed pyridine.

### Location of complexes

The diameters of the VO<sup>2+</sup>-picolinate complexes are larger than the zeolite-cage free-aperture (*ca.* 0.74 nm), so that the complexes cannot effectively penetrate into zeolite, but they are small enough to be confined in the large cavity (*id ca.* 1.2 nm) as shown in Fig. 3. Hence, the location of the complexes depends strongly on the preparation procedure. Table 2 shows XRF data for vanadium bulk concentration in the zeolite before and after Soxhlet extraction. Surface-bound complexes in the VO(pic)<sub>2</sub>-NaY (IM) sample prepared by an impregnation method were mainly removed by Soxhlet extraction, as shown in Table 2. On the other hand, negligible extractability of vanadium complexes in the VO(pic)<sub>2</sub>-NaY (SB) sample and the other (SB) samples prepared by the flexible ligand method indicates intrazeolitic location of complexes. Two other reliable estimates of the location of the complexes were obtained by XRD and from comparative analysis of XPS and XRF data.

XRD patterns for (a) NaY zeolite, (b) VO(pic)<sub>2</sub>-NaY (IM), (c) VO<sup>2+</sup>-NaY and (d) VO(pic)<sub>2</sub>-NaY (SB) samples are shown in Fig. 4. There was no significant loss in zeolite crystallinity for impregnated or encapsulated VO(pic)<sub>2</sub>-NaY samples as compared with the crystallinity of NaY zeolite. Note that the impregnated (IM) sample showed no additional feature which can be ascribed to a crystalline phase of vanadium compounds. Analysis of XRD patterns can supply information about the location of extraframework species such as charge-compensating cations and guest molecules in the zeolite pore system.<sup>24,25</sup> Qualitative information about site occupancies can be obtained from comparison of the relative intensities of selected XRD lines.<sup>26,27</sup> Quayle and Lunsford suggested that a relationship exists between the relative intensities of 331, 311 and 220 XRD peaks and cation location in faujasite-type zeolites.<sup>26</sup> If  $I_{331} > I_{220} > I_{311}$ , sodium cations are randomly distributed within the lattice, but the cations are assumed to be located at sites II and I if  $I_{331} > I_{311} > I_{220}$ . The XRD patterns (b) and (c) in Fig. 4 are similar to the pattern (a).

**Table 2** XRF and XPS data for selected NaY zeolite supported vanadium complexes

sample	Si/V ratio		
	XPS	XRF	
		before Soxhlet extraction	after Soxhlet extraction
VO <sup>2+</sup> -NaY	50	14	—
VO(pic) <sub>2</sub> -NaY (SB)	119	14	20
VO(pic) <sub>2</sub> -NaY (IM)	18	30	300
VO(Bupic) <sub>2</sub> -NaY (SB)	73	14	18
VO(Bupic) <sub>2</sub> -NaY (IM)	17	34	—
VO(Qpic) <sub>2</sub> -NaY (SB)	139	14	18
VO(Qpic) <sub>2</sub> -NaY (IM)	15	30	—

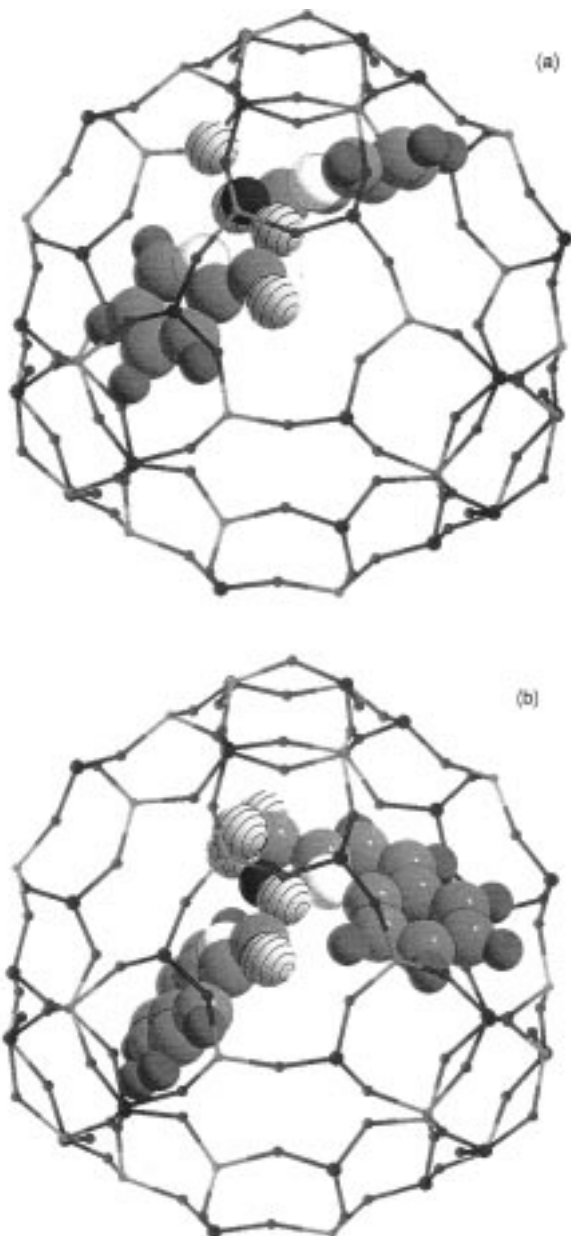


**Fig. 3** Computer graphic view of (a)  $\text{VO}(\text{pic})_2$  and (b)  $\text{VO}(\text{Qpic})_2$  in NaY supercage as created by Cerius<sup>2</sup> v1.6 with open force field burchart 1.01-universal 1.01

Thus, retention of the random location of sodium cations within the zeolite lattice is assumed, upon impregnation of the NaY zeolite with  $\text{VO}(\text{pic})_2 \cdot \text{H}_2\text{O}$  and ion exchange with  $\text{VO}^{2+}$ . However, analysis of the XRD pattern for the  $\text{VO}(\text{pic})_2$ -NaY (SB) sample reveals that complex formation is accompanied by significant cation redistribution. We pre-

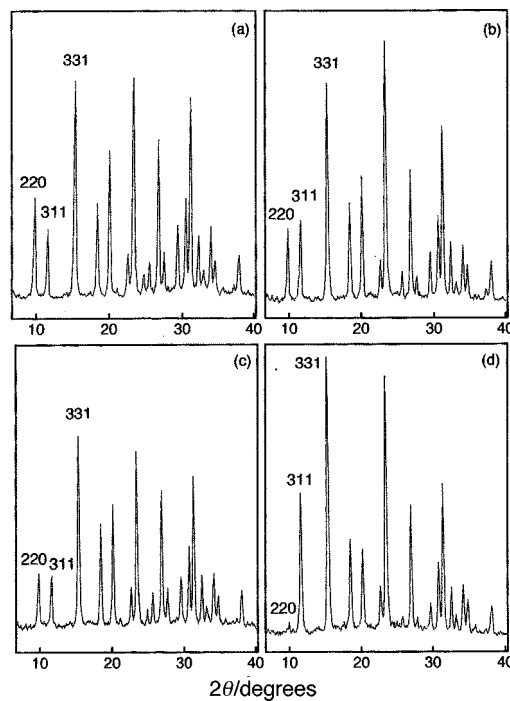


**Fig. 4** XRD patterns for (a) NaY, (b) impregnated  $\text{VO}(\text{pic})_2$ -NaY (IM) zeolite, (c)  $\text{VO}^{2+}$ -NaY and (d)  $\text{VO}(\text{pic})_2$ -NaY (SB) zeolite

sumed, therefore, that the large molecules of the  $\text{VO}(\text{pic})_2$  complex displaced the sodium cations, located in the supercages, from their original positions. Such intensity variations have been found for a variety of 'ship-in-a-bottle' systems, while complexes located on the external surface influence to a lesser extent.<sup>14,26,28,29</sup> Note that, in XRD patterns, the line 222, that could be ascribed to the antisymmetric character of the charge distribution with respect to the supercage centre,<sup>28</sup> is absent.

The location of the complexes in the zeolite cages is also suggested from a combination of XPS and XRF analyses.<sup>7</sup> XPS provides information about the relative concentrations of elements in the surface *ca.* 40–50 Å-thick layers of the sample (*ca.* 1% of the crystal), while XRF allows one to estimate bulk concentrations of the sample. It was found, from comparison of the signal intensities of the V  $2p_{3/2}$  level for the encapsulated samples (SB) and impregnated samples (IM), that the  $\text{VO}(\text{pic})_2$ -NaY (IM) sample had a higher complex concentration at the surface than the  $\text{VO}(\text{pic})_2$ -NaY (SB) sample (Table 2). The XPS measurements were carried out for various  $\text{VO}^{2+}$ -picolinate samples, and the surface concentration ratios (Si/V) are listed in Table 2. Obviously, the impregnated samples (IM) possess much higher vanadium concentrations at the external surfaces than the encapsulated samples (SB), despite lower vanadium loading of the impregnated samples. For example, the  $\text{VO}(\text{Qpic})_2$ -NaY (SB) sample shows an eight-fold lower surface concentration (XPS) than the bulk concen-

**Table 3** Binding energy (eV) for crystalline and NaY zeolite supported vanadium complexes

state	$\text{VO}(\text{pic})_2 \cdot \text{H}_2\text{O}$	$\text{VO}(\text{pic})_2$ -NaY (SB)	$\text{VO}(\text{pic})_2$ -NaY (IM)	$\text{VO}^{2+}$ -NaY
V $2p_{3/2}$	516.5	516.6	516.7	516.4
O 1s	532.0	532.2	532.2	532.2
N 1s	400.2	400.2	400.2	—
C 1s (C—C)	285.1	285.0	284.9	—
(O—C=O)	288.5	288.5	288.5	—
Si 2s	—	154.0	154.0	154.0
Si 2p	—	102.8	102.9	103.1
Al 2p	—	74.3	74.6	74.6
Na 1s	—	1072.8	1073.1	1073.1

tration (XRF), as shown in Table 2. However, the VO(Qpic)<sub>2</sub>-NaY (IM) sample possesses surface-enriched vanadium species, as reflected by the much smaller Si/V ratio in XPS than that in XPS for the SB sample and in XRF for the IM sample. Interestingly, for all the encapsulated samples, the surface concentration of vanadium determined by XPS was lower than that for the VO<sup>2+</sup>-NaY precursor. This can be explained by migration of non-complexed vanadyl ions under the high-temperature synthesis conditions used in the flexible ligand method.

In addition to the information about location of the complexes, some preliminary information about the states of both zeolite support and complexes was obtained from the XPS data. Table 3 lists the binding energies for V 2p<sub>3/2</sub>, O 1s, N 1s, C 1s, Si 2s, Si 2p, Al 2p, and Na 1s in various vanadium samples. The vanadium samples exhibited similar binding energies. At least two different kinds of carbon atoms (C—C 285.1 eV and O—C=O 288.5 eV) and the only kind of nitrogen atom (400.2 eV) were observed in the supported VO(pic)<sub>2</sub>-NaY samples (SB and IM), similar to the result for VO(pic)<sub>2</sub>·H<sub>2</sub>O. Thus the chemical states of vanadium atom and the picolinate ligand in the encapsulated samples (SB) are not different from that of the unsupported complex.

### Structure of complexes

The structure of encapsulated complexes formed by interaction of ligands with intrazeolitic transition metal ions is generally affected by specific conditions inside the zeolite framework, such as high electrostatic field and spatial restriction. In the present study the NaY encapsulated vanadium picolinate complex, as a representative sample among the three SB samples synthesized, was characterized by means of EPR, EXAFS, XANES, FTIR, and UV-VIS spectroscopies.

FTIR spectra of the encapsulated VO(pic)<sub>2</sub>-NaY (SB), VO(Bupic)<sub>2</sub>-NaY (SB), and VO(Qpic)<sub>2</sub>-NaY (SB) samples exhibited a strong band at ca. 1380–1390 cm<sup>-1</sup> and doublet bands at 1440–1490 cm<sup>-1</sup>, which are characteristic of picolinate species.<sup>30</sup> The band at ca. 1530 cm<sup>-1</sup> for the VO(pic)<sub>2</sub>-NaY (SB) sample before Soxhlet extraction, which is attributable to picolinic acid, almost disappeared after Soxhlet extraction for 60 h. The FTIR data for a series of the picolinate species are summarized in Table 4. No additional lines that could be ascribed to coordination modes different from bidentate were observed. The peak positions for VO(pic)<sub>2</sub>-NaY (SB) are similar to those for crystalline VO(pic)<sub>2</sub> complex and VO(pic)<sub>2</sub>-NaY (IM), which can be considered as indirect evidence for the bis-picolinate structure. On the other hand, the peak positions for the encapsulated vanadium complexes with substituted picolinic acids shifted to a larger extent. Thus, the peak positions are only slightly influenced by location of the complexes (SB and IM), but are changed by the nature of the picolinic ligand. This can be explained by changes in V-site geometry imposed by trapping of the vanadium picolinate complexes in the zeolite supercages. Such

changes may be caused by distortion of the encapsulated complexes inside the zeolite supercages or by a difference in coordination by the —OH groups of the zeolite.

UV-VIS diffuse reflectance spectra for various VO(pic)<sub>2</sub>-NaY samples are depicted in Fig. 5. The VO(pic)<sub>2</sub>-NaY (SB) sample (b) showed bands at 740, 560 and 370 nm assigned to the electronic transitions b<sub>2</sub> → e\*, b<sub>2</sub> → b<sub>1</sub>\*, and b<sub>2</sub> → 1a<sub>1</sub>\*, respectively, which resembled the bands for VO<sup>2+</sup>-picolinate complex in solution (730, 560 and 365 nm).<sup>31</sup> The band at ca. 270 nm is attributed to ligand π → π\* transition overlapped with LMCT of O to V<sup>4+</sup>. Note that the encapsulated VO(pic)<sub>2</sub>-NaY samples dried at room temperature in vacuum (c) and treated at 413 K for 10 h in a flow of He (b) showed similar spectra. However, there is a distinct difference in the spectra (d) and (e) between the impregnated VO(pic)<sub>2</sub>-NaY samples dried at room temperature and treated at 413 K. Impregnated VO(pic)<sub>2</sub>-NaY sample, after vacuum drying, exhibited bands at 670, 530(sh) and 270 nm [Fig. 5 (e)], while the VO(pic)<sub>2</sub>-NaY (IM) sample after heat treatment in a flow of He showed bands at 745, 550 and 273 nm [Fig. 5(d)]. The difference in the behaviour of the impregnated and encapsulated samples provides additional evidence about the location of the VO(pic)<sub>2</sub> complexes in the samples (SB and IM). The post-synthesis heat treatment aimed to remove adsorbed pyridine and to decompose the adduct of vanadium picolinate with pyridine which might be formed during Soxhlet extraction or the impregnation procedure. Indeed, the diffuse reflectance spectra for the impregnated sample changed from Fig. 5 (e) to (d) on heat treatment, which reflects the decomposition

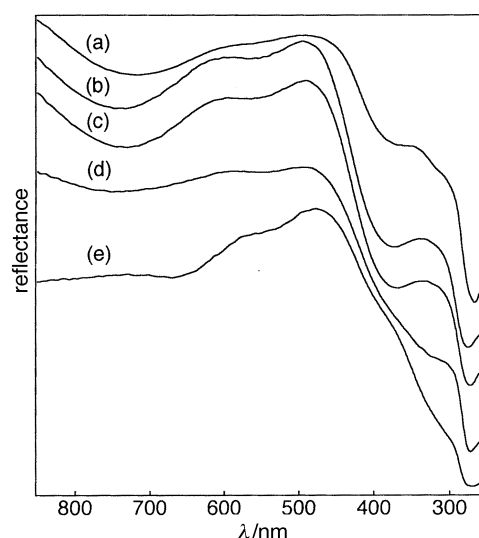


**Fig. 5** Diffuse reflectance spectra of VO(pic)<sub>2</sub>-NaY samples (referenced to NaY): (a) physical mixture of NaY and VO(pic)<sub>2</sub>·H<sub>2</sub>O, (b) VO(pic)<sub>2</sub>-NaY (SB) calcined in a flow of He (413 K for 10 h), (c) VO(pic)<sub>2</sub>-NaY (SB) dried in vacuum (298 K for 4 h), (d) VO(pic)<sub>2</sub>-NaY (IM) calcined in a flow of He (413 K for 10 h) and (e) VO(pic)<sub>2</sub>-NaY (IM) dried in vacuum (298 K for 4 h)

**Table 4** UV-VIS diffuse reflectance and FTIR spectral data for characterization of vanadium species

	VO(pic) <sub>2</sub> -NaY (SB)	VO(pic) <sub>2</sub> -NaY (IM)	VO(pic) <sub>2</sub> ·H <sub>2</sub> O	VO(pic) <sub>2</sub> in solution	VO(Bupic) <sub>2</sub> -NaY (SB)	VO(Qpic) <sub>2</sub> -NaY (SB)
FTIR (ν/cm <sup>-1</sup> )	1573	1570	1568		—	1567
	1480	1478	1480		1488	1488
	1454	1449	1450	—	1468	1466
	1389	1389	1389		1381	1379
	1299	1297	1297		1304	1303
	—	1262	1264		1263	1267
UV-VIS diffuse reflectance (λ/nm)	740	745	720	730		755
	560	550	560	560	—	320
	370	273	370	365		
	275		266			

of the  $\text{VO}(\text{pic})_2(\text{py})$  adduct. On the other hand, the same treatment did not lead to any visible change in the spectra for the encapsulated samples [Fig. 5(c) and (b)]. It is, therefore, possible to suppose that the formation of  $\text{VO}(\text{pic})_2(\text{py})$  is suppressed by spatial restriction, since the  $\text{VO}(\text{pic})_2$  complexes are located inside the zeolite supercage.

Fig. 6 shows vanadium K-edge XANES spectra of the  $\text{VO}(\text{pic})_2\text{-NaY}$  (IM) and  $\text{VO}(\text{pic})_2\text{-NaY}$  (SB) samples calcined in a flow of He (413 K for 10 h) as well as of reference compounds  $\text{VO}(\text{pic})_2 \cdot \text{H}_2\text{O}$  and  $\text{VO}(\text{pic})_2(\text{py})$ . The pre-edge and near-edge features were almost the same in position and intensity for the impregnated and encapsulated  $\text{VO}(\text{pic})_2\text{-NaY}$  samples and similar to those of  $\text{VO}(\text{pic})_2 \cdot \text{H}_2\text{O}$ . The pre-edge peak position was higher by *ca.* 4.0 eV than that for vanadium foil (not shown). These results indicate an oxidation state of  $\text{V}^{4+}$ . Comparison of the XANES spectra of the  $\text{VO}(\text{pic})_2\text{-NaY}$  (SB) sample with the corresponding spectra for well defined vanadium compounds reveals square pyramidal or distorted octahedral coordination around the vanadium site for the encapsulated SB sample.<sup>32</sup>

The Fourier transforms of the EXAFS data for the vanadium picolinate species are shown in Fig. 7. The difference in the Fourier transforms between  $\text{VO}(\text{pic})_2\text{-NaY}$  (IM) and

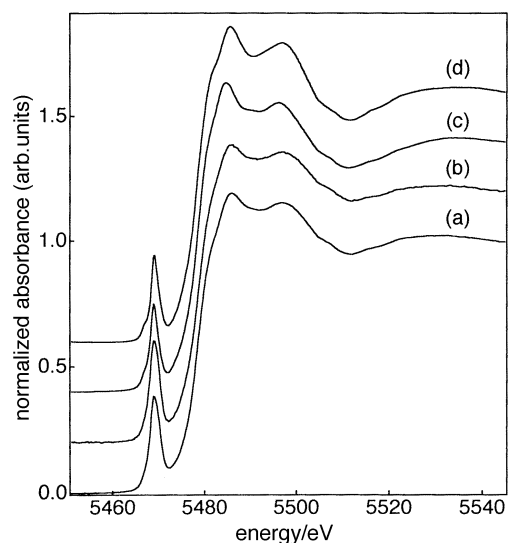


Fig. 6 Vanadium K-edges XANES of (a)  $\text{VO}(\text{pic})_2\text{-NaY}$  (IM), (b)  $\text{VO}(\text{pic})_2\text{-NaY}$  (SB), (c)  $\text{VO}(\text{pic})_2 \cdot \text{H}_2\text{O}$ , and (d)  $\text{VO}(\text{pic})_2(\text{py})$

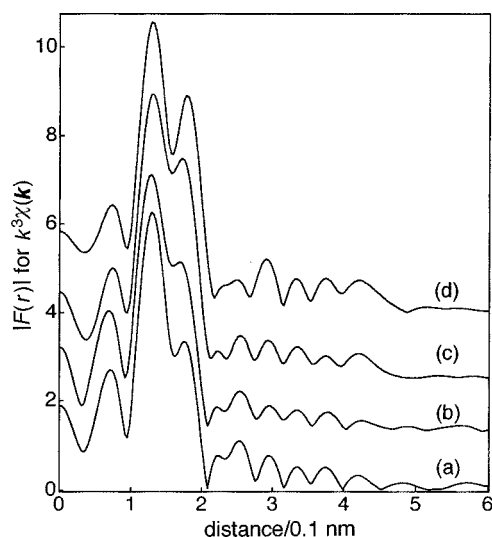


Fig. 7  $k^3$ -weighted Fourier transforms of EXAFS data for: (a)  $\text{VO}(\text{pic})_2\text{-NaY}$  (IM), (b)  $\text{VO}(\text{pic})_2\text{-NaY}$  (SB), (c)  $\text{VO}(\text{pic})_2 \cdot \text{H}_2\text{O}$ , and (d)  $\text{VO}(\text{pic})_2(\text{py})$

$\text{VO}(\text{pic})_2\text{-NaY}$  (SB) was related to the intensity change in the second shell. The second peak developed more with the reference complexes  $\text{VO}(\text{pic})_2 \cdot \text{H}_2\text{O}$  and  $\text{VO}(\text{pic})_2(\text{py})$  which have coordination of  $\text{H}_2\text{O}$  and pyridine in the axial position [Fig. 7 (c) and (d)]. The encapsulated  $\text{VO}^{2+}$ -picolinate complex may interact with the wall of the zeolite supercage, probably through a zeolite hydroxy group which coordinates to an axial position of the vanadium complex.

The most useful information about the  $\text{VO}^{2+}$  coordination sphere can be obtained from an EPR study.<sup>33,34</sup> To elucidate the change in coordination of the vanadium atom, the EPR spectra were recorded for the ion-exchanged  $\text{VO}^{2+}\text{-NaY}$  precursor as well as for the zeolite-supported vanadium picolinate complexes (Fig. 2 and Table 1). All the samples exhibited hyperfine splitting of two sets of eight lines, which reflects an unpaired electron density on the vanadium ion and an axial symmetry of its ligand field, and can be treated in terms of parallel and perpendicular components of the  $g$  and  $A$  values.

The  $\text{VO}(\text{pic})_2\text{-NaY}$  (SB) sample showed disappearance of the  $\text{VO}^{2+}\text{-NaY}$  zeolite signal ( $g_{\parallel} = 1.911$ ,  $g_{\perp} = 1.996$ ,  $A_{\parallel} = 205.8$  G and  $A_{\perp} = 85.4$  G) and appearance of a new signal with  $g_{\parallel} = 1.945$ ,  $g_{\perp} = 1.996$ ,  $A_{\parallel} = 175.3$  G and  $A_{\perp} = 67.1$  G. These  $g$  and  $A$  values are correlated with distorted octahedral vanadyl species in the  $\text{VO}(\text{pic})_2\text{-NaY}$  (SB) sample. On the other hand, the  $\text{VO}(\text{pic})_2\text{-NaY}$  (IM) sample showed superposition of two EPR signals with different parameters. One of them is a broad signal with  $g \approx 1.95$ , indicating the formation of crystalline  $\text{VO}(\text{pic})_2$  on the external surface of the zeolite.<sup>35</sup> The other is an anisotropic 16-line signal similar to that for the  $\text{VO}(\text{pic})_2\text{-NaY}$  (SB) sample. The similarity of the EPR parameters for the  $\text{VO}(\text{pic})_2\text{-NaY}$  (SB) and  $\text{VO}(\text{pic})_2\text{-NaY}$  (IM) samples suggests the absence of significant structural distortion of the zeolite-encapsulated  $\text{VO}(\text{pic})_2$  complex. Upon complexation with picolinic acids, a decrease in  $A$  values was observed with a simultaneous increase in  $g_{\parallel}$ . This is interpreted in terms of a decrease in the  $\text{V}=\text{O}$  bond covalency ( $\Delta g_{\parallel} > 0$ ) while covalency of the  $\text{V}$ -ligand bond increases ( $\Delta A < 0$ ).<sup>20,21</sup>

Generally, introduction of substituents on the ligand periphery does not significantly affect the complex geometry and, in consequence, the EPR parameters. On the other hand, the correlation between donor number of a solvent and  $A$  and  $g$  values has been reported.<sup>36</sup> Significant deviations of the EPR parameters were observed for  $\text{VO}(\text{Bupic})_2\text{-NaY}$  (SB) and  $\text{VO}(\text{Qpic})_2\text{-NaY}$  (SB) in comparison with those for  $\text{VO}(\text{pic})_2\text{-NaY}$  (SB) (Table 1). The difference is reasonably ascribed to a difference in sixth-site coordination of the encapsulated vanadium picolinate. Actually, coordination with the zeolite OH group may be weakened due to spatial restriction imposed by encapsulation. A computer modelling study on the location of the vanadium picolinate in the NaY supercage indicated that  $\text{VO}(\text{Qpic})_2$  preferentially occupies the centre of the supercage, whereas the location of  $\text{VO}(\text{pic})_2$  in the supercage is less restricted and the complex can come close to the wall of the supercage (Fig. 3).

#### Stability of the $\text{VO}(\text{pic})_2\text{-NaY}$ (SB) complex and gas-phase oxidation

Thermal decomposition of the vanadyl bis-picolinate complex has been demonstrated to occur through dimeric species.<sup>37</sup> Hence, we expected increased stability for the encapsulated complexes dispersed in the supercages in comparison with the impregnated sample, which could allow us to use such materials as catalysts under oxidation conditions.

Under non-oxidative conditions, thermal decomposition of pyridine-2-carboxylate proceeds *via* decarboxylation to yield  $\text{CO}_2$  and the corresponding aromatic amine. Temperature-

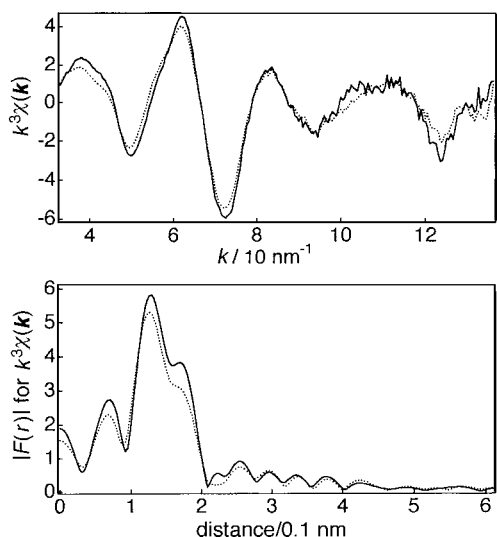


**Fig. 8**  $k^3$ -weighted vanadium K-edge EXAFS and Fourier-transform data for encapsulated  $\text{VO}(\text{pic})_2\text{-NaY}$  (SB) samples: (—) as synthesized; (·····) calcined in air at 523 K for 3 h

programmed decomposition (TPD) experiments were carried out in a flow of He at a heating rate of  $2 \text{ K min}^{-1}$ . The TPD spectra for  $\text{CO}_2$  evolution showed maxima at 633, 633 and 593 K for the encapsulated  $\text{VO}(\text{pic})_2$ ,  $\text{VO}(\text{Bupic})_2$ , and  $\text{VO}(\text{Qpic})_2$  complexes, respectively. These values were similar to those for the impregnated samples. However, under oxidative conditions, the stability of the complexes was found to depend strongly on the complex location. Fig. 8 shows EXAFS data for  $\text{VO}(\text{pic})_2\text{-NaY}$  (SB) before and after calcination in oxygen at 523 K for 3 h. The similarity in the Fourier transforms and the raw EXAFS data for both samples indicates the retention of the bis-picolinate structure of the complex. In contrast, the  $\text{VO}(\text{pic})_2\text{-NaY}$  (IM) sample showed definite changes in EXAFS oscillations and Fourier transforms (Fig. 9). This might have been caused by oxidative destruction of the  $\text{VO}(\text{pic})_2$  complex to vanadium(v) oxide species. This suggestion agrees with the absence of any band in the FTIR spectra characteristic of picolinato ligand as well as the complete disappearance of the  $\text{V}^{4+}$  signal in the EPR spectra. The difference in the behaviour of the impregnated and encapsulated materials seems to be due to easier destruction of the  $\text{VO}(\text{pic})_2$  complex in the case of  $\text{VO}(\text{pic})_2\text{-NaY}$

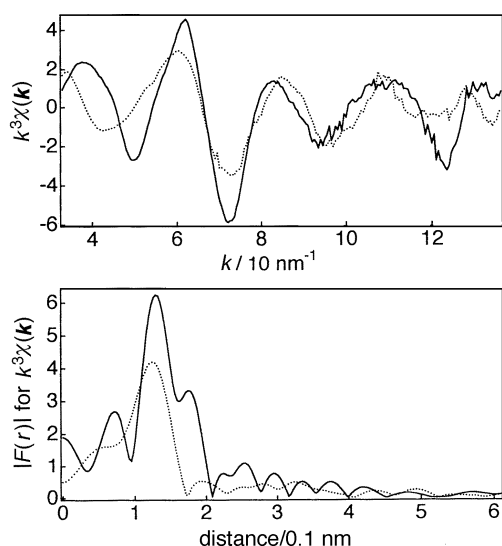


**Fig. 9**  $k^3$ -weighted vanadium K-edge EXAFS and Fourier-transform data for impregnated  $\text{VO}(\text{pic})_2\text{-NaY}$  (IM) samples: (—) as synthesized, (·····) calcined in air at 523 K for 3 h

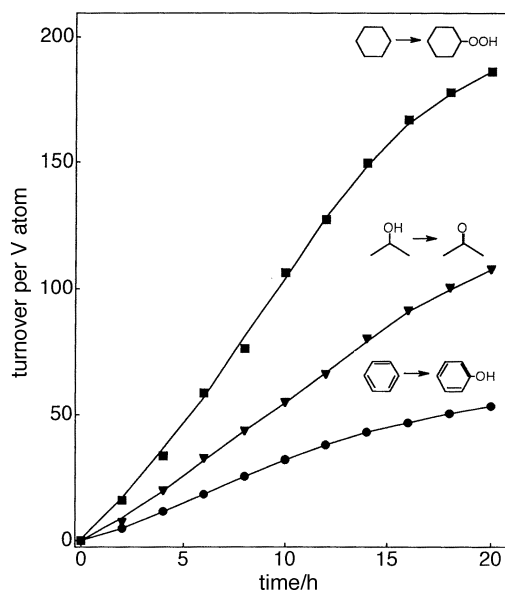


**Fig. 10** Product accumulation in catalytic oxidation with encapsulated  $\text{VO}(\text{pic})_2\text{-NaY}$  (SB) catalyst. Reaction conditions: acetonitrile, 20 ml; substrate (cyclohexane, isopropyl alcohol, benzene), 6 mmol;  $\text{H}_2\text{O}_2$ -urea adduct, 20 mmol;  $\text{VO}(\text{pic})_2\text{-NaY}$  (SB), 0.04 g ( $1 \times 10^{-5}$  mol), 313 K.

(IM) sample through dimeric species that are hardly formed when the complex is encapsulated.

Thus, the encapsulated  $\text{VO}(\text{pic})_2$ ,  $\text{VO}(\text{Bupic})_2$  and  $\text{VO}(\text{Qpic})_2$  complexes were found to be stable up to 573 K in air. However, despite the relatively high stability of the encapsulated complexes, attempts to use these materials as catalysts for gas-phase oxidation reactions such as the selective oxidation of light alkanes and alkenes, below 573 K were unsuccessful.

#### Catalytic performance for heterogeneous liquid-phase oxidation

Catalysis of vanadium peroxo complexes containing pyridinecarboxylato ligands in solutions has been studied by Mimoun *et al.*<sup>14</sup> and Shul'pin *et al.*<sup>38,39</sup> It was observed that these compounds can effectively catalyse hydroxylation of aromatic and aliphatic hydrocarbons as well as the oxidation of alcohols. We found that the encapsulated  $\text{VO}(\text{pic})_2$  complex detaches from the zeolite when treated with 30%  $\text{H}_2\text{O}_2$  solution. Hence, in the present study, the preliminary catalytic oxidations were carried out under anhydrous conditions to suppress the leaching. It was found that cyclohexane, isopropyl alcohol and benzene were catalytically oxidized by  $\text{VO}(\text{pic})_2\text{-NaY}$  (SB) in the presence of urea hydrogen peroxide adduct in acetonitrile to cyclohexyl hydroperoxide, acetone and phenol, respectively. The reaction profiles are shown in Fig. 10, and demonstrate that the encapsulated  $\text{VO}(\text{pic})_2\text{-NaY}$  (SB) sample is an effective catalyst for the selective oxidation of hydrocarbons. Details at the catalytic performance will be reported separately.<sup>40</sup>

#### Conclusions

Vanadium picolinate complexes  $\text{VO}(\text{pic})_2\text{-NaY}$  (SB),  $\text{VO}(\text{Bupic})_2\text{-NaY}$  (SB), and  $\text{VO}(\text{Qpic})_2\text{-NaY}$  (SB) encapsulated inside NaY zeolite supercages were synthesized by the flexible ligand method that involved treatment of a  $\text{VO}^{2+}\text{-NaY}$  zeolite with molten picolinic acids followed by Soxhlet extraction to remove excess ligands and complexes located on external surfaces of the zeolite. Careful characterization of the encapsulated species by EXAFS, XANES, FTIR, EPR and UV-VIS spectroscopies proved the formation of bis-picolinate complexes with distorted octahedral coordination around vanadium. The coordination of zeolite OH groups to the

vanadium complexes was used to explain the difference in spectroscopic properties of the impregnated and encapsulated samples as well as the significant size dependence of the EPR parameters for the encapsulated samples. It was suggested by XRD, as well as by comparative XPS–XRF, studies that the complexes were encapsulated in the zeolite supercages. The encapsulated VO(pic)<sub>2</sub> complex retained solution-like activity in the selective oxidation of hydrocarbons.

This work was supported by CREST (Core Research for Evolutional Science and Technology) of JST (Japan Science and Technology Corporation).

## References

- 1 P. B. Venuto, *Microporous Mater.*, 1994, **2**, 297.
- 2 D. R. C. Huybrechts, R. F. Parton and P. A. Jacobs, *Stud. Surf. Sci. Catal.*, 1991, **60**, 225.
- 3 G. Bellussi and M. S. Rigutto, *Stud. Surf. Sci. Catal.*, 1994, **85**, 177.
- 4 J. Weitkamp, U. Weiß and S. Ernst, *Stud. Surf. Sci. Catal.*, 1995, **94**, 363.
- 5 R. A. Sheldon, J. D. Chen, J. Dakka and E. Neeleman, *Stud. Surf. Sci. Catal.*, 1994, **82**, 515.
- 6 D. E. De Vos, F. Thibault-Starzyk, P. P. Knops-Gerrits, R. F. Parton and P. A. Jacobs, *Macromol. Symp.*, 1994, **80**, 157.
- 7 K. J. Balkus Jr. and A. G. Gabrielov, *J. Inclusion Phenom. Mol. Recognit. Chem.*, 1995, **21**, 159.
- 8 D. R. Corbin and N. Herron, *J. Mol. Catal.*, 1994, **86**, 343.
- 9 B. Romanovsky, *Macromol. Symp.*, 1994, **80**, 185.
- 10 V. Yu. Zakharov, O. M. Zakharova, B. V. Romanovsky and R. E. Mardaleishvili, *React. Kinet. Catal. Lett.*, 1977, **6**, 133.
- 11 A. Butler, M. J. Clague and G. E. Meister, *Chem. Rev.*, 1994, **94**, 625.
- 12 K. A. Jorgensen, *Chem. Rev.*, 1989, **3**, 431.
- 13 V. Conte, F. Di Furia and G. Licini, *Appl. Catal. A*, 1997, **157**, 335.
- 14 K. J. Balkus Jr., A. K. Khanmamedova, K. M. Dixon and F. Bedioui, *Appl. Catal. A*, 1996, **143**, 159.
- 15 P. P. Knops-Gerrits, C.A. Trujillo, B. Z. Zhan, X. Y. Li, P. Rouxhet and P.A. Jacobs, *Top. Catal.*, 1996, **3**, 437.
- 16 H. Mimoun, L. Saussine, E. Daire, M. Postel, J. Fischer and R. Weiss, *J. Am. Chem. Soc.*, 1983, **105**, 3101.
- 17 A. Kozlov, K. Asakura and Y. Iwasawa, *Chem. Lett.*, 1997, 313.
- 18 K. Maruszewski, D. P. Strommen, K. Handrich and R. Kincaid, *Inorg. Chem.*, 1991, **30**, 4579.
- 19 R. L. Dutta and S. Ghosh, *J. Indian Chem. Soc.*, 1967, **44**, 271.
- 20 G. Martini, M. F. Ottaviani and G. L. Seravalli, *J. Phys. Chem.*, 1975, **79**, 1716.
- 21 H. J. Stoklosa, J. R. Wasson and B. J. McCormick, *Inorg. Chem.*, 1974, **13**, 592.
- 22 *Handbook of X-ray Photoelectron Spectroscopy*, JEOL, Tokyo, 1991, p. 12.
- 23 C. A. Trujillo, U. N. Uribe, P. P. Knops-Gerrits, L. A. A. Oviedo and P. A. Jacobs, *J. Catal.*, 1997, **168**, 1.
- 24 C. Kirschhock and H. Fuess, *J. Chem. Soc., Faraday Trans.*, 1995, **91**, 1813.
- 25 Z. A. Kaszkur, R. H. Jones, D. Waller, C. R. A. Catlow and J. M. Thomas, *J. Phys. Chem.*, 1993, **97**, 426.
- 26 W. H. Quayle and J. H. Lunsford, *Inorg. Chem.*, 1982, **21**, 97.
- 27 J. M. Thomas, C. Williams and T. Rayment, *J. Chem. Soc., Faraday Trans. 1*, 1988, **84**, 2915.
- 28 Y. Okamoto, H. Katsuyama, K. Yoshida, K. Nakai, M. Matsuo, Y. Sakamoto, J. Yu and O. Terasaki, *J. Chem. Soc., Faraday Trans.*, 1996, **92**, 4647.
- 29 G. Vankó, Z. Homonnay, S. Nagy, A. Vértés, G. Pál-Borbély and H. K. Beyer, *Chem. Commun.*, 1996, 785.
- 30 M. Paris, G. Thomas and J-C. Merlin, *Bull. Soc. Chim. Fr.*, 1961, 707.
- 31 M. Paris and J-C. Merlin, *Bull. Soc. Chim. Fr.*, 1962, 800.
- 32 J. Wong, F. W. Lytle, R. P. Messmer and D. H. Maylotte, *Phys. Rev. B*, 1984, **30**, 5596.
- 33 M. Petrás and B. Wichterlová, *J. Phys. Chem.*, 1992, **96**, 1805.
- 34 A. Jezierski and J. B. Raynor, *J. Chem. Soc., Dalton Trans.*, 1981, 1.
- 35 G. Centi, S. Perathoner, F. Trifiró, A. Aboukais, C. F. Aïssi and M. Guelton, *J. Phys. Chem.*, 1992, **96**, 2617.
- 36 S. H. Cheng, S. R. Sheen, C. P. Cheng and C. T. Chang, *Inorg. Chim. Acta*, 1990, **171**, 21.
- 37 R. L. Dutta, S. Ghosh and W. W. Wendlandt, *J. Indian Chem. Soc.*, 1967, **44**, 811.
- 38 G. B. Shul'pin and G. Süß-Fink, *J. Chem. Soc., Perkin Trans. 2*, 1995, 1459.
- 39 G. B. Shul'pin, D. Attanasio and L. Suber, *J. Catal.*, 1993, **142**, 147.
- 40 A. Kozlov, K. Asakura and Y. Iwasawa, to be published.

Paper 7/06679A; Received 15th September, 1997